Measurement of the neutron capture cross section of the *s*-only isotope ^{204}Pb from 1 eV to 440 keV

C. Domingo-Pardo,[1,2,*] U. Abbondanno,[3] G. Aerts,[4] H. Álvarez-Pol,[5] F. Alvarez-Velarde,[6] S. Andriamonje,[4] J. Andrzejewski,[7] P. Assimakopoulos,[8] L. Audouin,[1] G. Badurek,[9] P. Baumann,[10] F. Bečvář,[11] E. Berthoumieux,[4] S. Bisterzo,[1,12] F. Calviño,[13] D. Cano-Ott,[6] R. Capote,[14,15] C. Carrapiço,[16] P. Cennini,[17] V. Chepel,[18] E. Chiaveri,[17] N. Colonna,[19] G. Cortes,[13] A. Couture,[20] J. Cox,[20] M. Dahlfors,[17] S. David,[21] I. Dillmann,[1,38] R. Dolfini,[22] W. Dridi,[4] I. Duran,[5] C. Eleftheriadis,[23] M. Embid-Segura,[6] L. Ferrant,[21] A. Ferrari,[17] R. Ferreira-Marques,[18] L. Fitzpatrick,[17] H. Frais-Koelbl,[24] K. Fujii,[3] W. Furman,[25] R. Gallino,[12] I. Goncalves,[18] E. Gonzalez-Romero,[6] A. Goverdovski,[26] F. Gramegna,[27] E. Griesmayer,[24] C. Guerrero,[6] F. Gunsing,[4] B. Haas,[28] R. Haight,[29] M. Heil,[1] A. Herrera-Martinez,[17] M. Igashira,[30] S. Isaev,[21] E. Jericha,[9] Y. Kadi,[17] F. Käppeler,[1] D. Karamanis,[8] D. Karadimos,[8] M. Kerveno,[10] V. Ketlerov,[17,26] P. Koehler,[31] V. Konovalov,[17,25] E. Kossionides,[32] M. Krtička,[11] C. Lamboudis,[23] H. Leeb,[9] A. Lindote,[18] I. Lopes,[18] M. Lozano,[15] S. Lukic,[10] J. Marganiec,[7] S. Marrone,[19] P. Mastinu,[27] A. Mengoni,[14,17] P. M. Milazzo,[3] C. Moreau,[3] M. Mosconi,[1] F. Neves,[18] H. Oberhummer,[9] M. Oshima,[33] S. O'Brien,[20] J. Pancin,[4] C. Papachristodoulou,[8] C. Papadopoulos,[34] C. Paradela,[5] N. Patronis,[8] A. Pavlik,[35] P. Pavlopoulos,[36] L. Perrot,[4] R. Plag,[1] A. Plompen,[37] A. Plukis,[4] A. Poch,[13] C. Pretel,[13] J. Quesada,[15] T. Rauscher,[38] R. Reifarth,[28] M. Rosetti,[39] C. Rubbia,[22] G. Rudolf,[10] P. Rullhusen,[37] J. Salgado,[16] L. Sarchiapone,[17] I. Savvidis,[23] C. Stephan,[21] G. Tagliente,[19] J. L. Tain,[2] L. Tassan-Got,[21] L. Tavora,[16] R. Terlizzi,[19] G. Vannini,[39] P. Vaz,[16] A. Ventura,[39] D. Villamarin,[6] M. C. Vincente,[6] V. Vlachoudis,[17] R. Vlastou,[34] F. Voss,[1] S. Walter,[1] H. Wendler,[17] M. Wiescher,[20] and K. Wisshak[1]

(n_TOF Collaboration)

[1]*Forschungszentrum Karlsruhe GmbH (FZK), Institut für Kernphysik, Germany*

[2]*Instituto de Física Corpuscular, CSIC-Universidad de Valencia, Spain*

[3]*Istituto Nazionale di Fisica Nucleare, Trieste, Italy*

[4]*CEA/Saclay-DSM, Gif-sur-Yvette, France*

[5]*Universidade de Santiago de Compostela, Spain*

[6]*Centro de Investigaciones Energeticas Medioambientales y Technologicas, Madrid, Spain*

[7]*University of Lodz, Lodz, Poland*

[8]*University of Ioannina, Ioannina, Greece*

[9]*Atominstitut der Österreichischen Universitäten, Technische Universität Wien, Vienna, Austria*

[10]*Centre National de la Recherche Scientifique/IN2P3-IReS, Strasbourg, France*

[11]*Charles University, Prague, Czech Republic*

[12]*Dipartimento di Fisica Generale, Università di Torino, Torino, Italy*

[13]*Universitat Politecnica de Catalunya, Barcelona, Spain*

[14]*International Atomic Energy Agency, NAPC-Nuclear Data Section, Vienna, Austria*

[15]*Universidad de Sevilla, Sevilla, Spain*

[16]*Instituto Tecnológico e Nuclear(ITN), Lisbon, Portugal*

[17]*CERN, Geneva, Switzerland*

[18]*LIP-Coimbra and Departamento de Fisica da Universidade de Coimbra, Coimbra, Portugal*

[19]*Istituto Nazionale di Fisica Nucleare, Bari, Italy*

[20]*University of Notre Dame, Notre Dame, Indiana, USA*

[21]*Centre National de la Recherche Scientifique/IN2P3-IPN, Orsay, France*

[22]*Università degli Studi Pavia, Pavia, Italy*

[23]*Aristotle University of Thessaloniki, Thessaloniki, Greece*

[24]*Fachhochschule Wiener Neustadt, Wiener Neustadt, Austria*

[25]*Joint Institute for Nuclear Research, Frank Laboratory of Neutron Physics, Dubna, Russia*

[26]*Institute of Physics and Power Engineering, Kaluga region, Obninsk, Russia*

[27]*Istituto Nazionale di Fisica Nucleare (INFN), Laboratori Nazionali di Legnaro, Legnaro, Italy*

[28]*Centre National de la Recherche Scientifique/IN2P3-CENBG, Bordeaux, France*

[29]*Los Alamos National Laboratory, Los Alamos, New Mexico, USA*

[30]*Tokyo Institute of Technology, Tokyo, Japan*

[31]*Oak Ridge National Laboratory, Physics Division, Oak Ridge, Tennessee, USA*

[32]*NCSR, Athens, Greece*

[33]*Japan Atomic Energy Research Institute, Tokai-mura, Japan*

[34]*National Technical University of Athens, Athens, Greece*

[35]*Institut für Isotopenforschung und Kernphysik, Universität Wien, Vienna, Austria*

[36]*Pôle Universitaire Léonard de Vinci, Paris La Défense, France*

[37]*CEC-JRC-IRMM, Geel, Belgium*

[38]*Department of Physics and Astronomy, University of Basel, Basel, Switzerland*

[39]*ENEA, Bologna, Italy*

[40]*Dipartimento di Fisica, Università di Bologna, and Sezione INFN di Bologna, Italy*
(Received 18 October 2006; published 19 January 2007)

The neutron capture cross section of ^{204}Pb has been measured at the CERN n_TOF installation with high resolution in the energy range from 1 eV to 440 keV. An R-matrix analysis of the resolved resonance region, between 1 eV and 100 keV, was carried out using the SAMMY code. In the interval between 100 keV and 440 keV we report the average capture cross section. The background in the entire neutron energy range was reliably determined from the measurement of a ^{208}Pb sample. Other systematic effects in this measurement were investigated and precisely corrected by means of detailed Monte Carlo simulations. We obtain a Maxwellian average capture cross section for ^{204}Pb at $kT = 30$ keV of 79(3) mb, in agreement with previous experiments. However our cross section at $kT = 5$ keV is about 35% larger than the values reported so far. The implications of the new cross section for the s-process abundance contributions in the Pb/Bi region are discussed.

DOI: 10.1103/PhysRevC.75.015806 PACS number(s): 25.40.Lw, 27.80.+w, 97.10.Cv

I. INTRODUCTION

The heaviest stable isotopes with masses $A = 204$–209 are synthesized by neutron capture reactions, the s and the r processes. According to the stellar model of Arlandini *et al.* [1], the s-process fraction of ^{204,206}Pb is mostly produced in thermally pulsing asymptotic giant branch (AGB) stars, the so-called main component of the s process. On the other hand, the galactic chemical evolution study of Travaglio *et al.* [2,3] showed that the heavier lead isotopes ^{207,208}Pb and bismuth are basically synthesized by early generation, low-metallicity, low-mass AGB stars. Bismuth is the last element synthesized by the slow process, thus further neutron captures on this isotope are recycled back to ^{206,207,208}Pb via α-decays.

The situation at the end of the s process is complicated due to branchings in the α-recycling at ^{210}Po ($t_{1/2} = 138$ d) and at ^{210m}Bi ($t_{1/2} = 3$ Myr). In this termination region, ^{204}Pb is the only of pure s-process origin, because it is shielded from the r process by its isobar ^{204}Hg. Therefore, ^{204}Pb is important for disentangling the complex Pb/Bi abundance pattern. The solar abundance and the cross section of ^{204}Pb need to be accurately known for a consistent determination of the s-process components of the Pb/Bi abundances, which provides a basis for constraining the complementary contributions from explosive r-process nucleosynthesis.

With an improved s-process part, the respective r components, which consist of the direct r-process yields as well as of the decay products from the α-unstable trans-bismuth region, could be more accurately determined [4]. The radiogenic fractions are important in order to consolidate the validity of the U/Th cosmochronometer [5–8]. The cross section of ^{204}Pb also enters into the calculation of the s-process branching at ^{204}Tl. Since this branching shows a strong temperature dependence, the abundance of ^{204}Pb represents an important test for AGB models, which exhibit strongly different neutron densities and temperatures in and between thermal pulses [9].

Thanks to improvements both in experimental techniques and detectors, difficulties in previous measurements of the (n, γ) cross section of ^{204}Pb [10] were significantly reduced. This concerns the investigated neutron energy range, which had been covered only for energies above 2.5 keV with the consequence that some important resonances were missed. It also concerns the correction for background from neutrons scattered in the sample, which had a strong effect on the capture width of broad resonances. The setup in previous experiments suffered from large scattering corrections with uncertainties of ∼50%. Apart from this problem, the remaining systematic uncertainties had been estimated to be ±5% [10].

The (n, γ) cross section measurement at the CERN n_TOF facility [11] has covered the full energy range between 1 eV and 1 MeV in a single experiment, and the corrections due to scattered neutrons became negligible for all resonances by using C_6D_6 detectors with reduced neutron sensitivity [12]. Furthermore, systematic uncertainties were improved to the level of 3% [13] by detailed Monte Carlo simulations of the experimental setup.

II. CROSS SECTION MEASUREMENT

The present measurement was carried out with a ^{204}Pb sample of 99.7% isotopic enrichment. At n_TOF, neutrons are produced by spallation reactions using a pulsed proton beam [6 ns (rms), 20 GeV/c] impinging on a lead block. A water layer around the lead target serves as moderator of the initially fast neutron spectrum, as well as coolant of the spallation target. Particularly relevant for this measurement was the low n_TOF duty cycle with a pulse repetition rate of 0.4 Hz, which allows us to cover a wide energy range from 1 MeV down to 1 eV. A further advantage of the present measurement is the small sample thickness of $n = 0.00376$ at/barn (see Table I). In this way, systematic effects due to multiple scattering and neutron self-absorption in the sample become rather low.

The sample was mounted on the ladder of an evacuated sample changer made from carbon fiber. In addition a thin gold sample (see Table I) was also regularly measured for absolute yield normalization via the saturated resonance technique [14], and an enriched ^{208}Pb sample, which has a negligibly small (n, γ) cross section with only few resonances in the investigated energy range, served for the the determination of the in-beam γ-ray background produced by neutron captures in the water moderator of the lead spallation target. Due to

*Corresponding author. Email address: cesar.domingo.pardo@cern.ch.

TABLE I. Sample characteristics (all samples were 20 mm in diameter).

Sample	Mass (g)	Thickness (at/barn)	Isotopic composition (%)
^{204}Pb	4.039	0.00376	99.7
^{208}Pb	12.53	0.01155	99.86
^{197}Au	0.768	0.00074	100

the relatively large cross section of ^{204}Pb, this background was only a minor difficulty for the present measurement.

Neutron capture events were registered via the prompt capture γ-ray cascade by a set of two C_6D_6 detectors, which were optimized with respect to neutron sensitivity [12]. The detectors were placed at 125° with respect to the direction of the neutron beam in order to minimize angular distribution effects as well as the background due to in-beam γ-rays. A schematic view of the experimental setup can be seen in Fig. 2 of Ref. [15]. The neutron flux $\Phi_n(E_n)$ was previously determined by measuring the well-known ^{235,238}U fission yields [16]. During the experiment it was determined by means of the saturated gold resonance at 4.9 eV measured with the gold sample, and it was also monitored by means of a monitor detector consisting of a thin ^{6}Li foil surrounded by a set of four silicon large detectors for recording the products of the ^{6}Li$(n,\alpha)^3$H reactions [17].

III. DATA ANALYSIS

Since the γ-ray efficiency of the C_6D_6 detectors is rather small, their response function needs to be appropriately weighted in order to achieve a cascade detection probability independent of the particular γ-ray registered. This is achieved by applying the pulse height weighting technique (PHWT) [18]. In the present analysis the weighting functions (WF) for the measured lead and gold samples were obtained via the Monte Carlo technique, following the procedure described in Refs. [13,15].

The experimental capture yield $Y^{\rm exp}$ can then be determined from the measured and weighted count rate (N^w),

$$Y^{\rm exp}(E_n) = f^t f^{\rm sat} \frac{N^w(E_n)}{\Phi_n(E_n) E_c(E_n)}, \qquad (1)$$

where E_c is the neutron capture energy, $f^{\rm sat}$ an absolute yield normalization factor determined from the analysis of the 4.9 eV saturated resonance in the gold runs, and f^t is a yield correction factor, which accounts for the effect of the threshold in the pulse height spectra of the C_6D_6 detectors. The latter correction factors f^t, which were obtained by Monte Carlo simulations as described in Refs. [13,15], were found to differ from unity by 3.1(3)% for resonances with spin $J = 1/2$ and by 3.6(3)% for $J = 3/2$ resonances. In the analysis of the unresolved resonance region we kept the same correction f^t as for $J = 1/2$ resonances. The treatment of the experimental background will be described in the two following sections.

TABLE II. Systematic uncertainties in the measured cross section of ^{204}Pb.

Effect	Uncertainty (%)
PHWT and yield normalization factors, $f^{\rm sat}$	<2
Background subtraction	1(10)[a]
Flux shape	2
Yield correction factors, f^t	0.3
Total systematic uncertainty	3 (10)[a]

[a]Values in brackets refer to the unresolved resonance region between 100 and 440 keV.

The systematic uncertainties of the present measurement are summarized in Table II.

IV. RESULTS IN THE RESOLVED RESONANCE REGION

In the resolved resonance region (RRR), the experimental yield (1) is described by means of the R-matrix formalism in terms of individual resonance parameters using an equation of the type

$$Y^{\rm exp} = B(E_n) + Y(E_\circ, \Gamma_n, \Gamma_\gamma). \qquad (2)$$

Where available, the neutron widths Γ_n from literature [19] have been used as input for the present analysis. The capture width Γ_γ of each observed resonance was fitted with the R-matrix code SAMMY [20], which includes also corrections for several experimental effects, e.g., for Doppler broadening, multiple neutron scattering and self-shielding in the sample. The background term $B(E_n)$ has been precisely determined from the concomitant (n,γ) measurement with a ^{208}Pb sample. Given the much lower capture cross section of ^{208}Pb, the C_6D_6 response function to in-beam γ-rays scattered by the ^{204}Pb sample was directly determined from the measured ^{208}Pb spectrum. The contribution from scattered γ-rays dominated the overall background in the present measurement by far.

In the interval from 1 eV to 30 keV, $B(E_n)$ was adjusted to a function of the type

$$B(E_n) = A_1 + \frac{A_2}{\sqrt{E_n}} + A_3\sqrt{E_n}. \qquad (3)$$

Between 30 and 100 keV the background showed systematic fluctuations, which could not be described by means of a single analytical function. Hence, the background was defined in that energy range by a pointwise numerical function, as illustrated in Fig. 1.

The capture widths, Γ_γ, obtained in this analysis are listed in Table III. Also, the capture kernels

$$K_r = \frac{2J+1}{2} \frac{\Gamma_\gamma \Gamma_n}{\Gamma_\gamma + \Gamma_n} \qquad (4)$$

are given for each case together with the respective uncertainties.

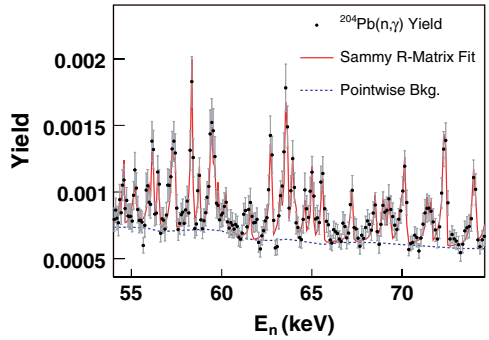

FIG. 1. (Color online) ^{204}Pb capture yield and pointwise background in the neutron energy region between 54 and 74 keV.

V. RESULTS IN THE UNRESOLVED RESONANCE REGION

The average capture yield $\langle Y(E_n)\rangle$ is related to the average capture cross section $\langle\sigma_\gamma(E_n)\rangle$ by

$$\langle Y(E_n)\rangle = n f^{\rm ms}(E_n)\langle\sigma_\gamma(E_n)\rangle, \qquad (5)$$

where n is the sample thickness in atoms per barn and $f^{\rm ms}(E_n)$ is the neutron self-shielding and multiple scattering correction. This correction was determined via the Monte Carlo technique using the code SESH [21]. In the considered region between 100 and 400 keV the correction factors $f^{\rm ms}(E_n)$ are practically constant as shown in Fig. 2.

The averaged cross sections $\langle\sigma_\gamma(E_n)\rangle$ are given in Table IV together with the respective statistical uncertainties. An overall systematic uncertainty of $\pm$10% has to be added in order to account for the systematic uncertainties of $f^{\rm ms}(E_n)$ and of the background subtraction in this energy range.

VI. IMPLICATIONS FOR THE *s*-PROCESS ABUNDANCE OF THE PB/BI ISOTOPES

Since ^{204}Pb is shielded from the r process by ^{204}Hg, the observed solar abundance of ^{204}Pb is only produced by the s-process branching at ^{204}Tl, which is very sensitive to stellar temperature. Furthermore, the abundance of ^{204}Pb is not affected by the α-recycling at the end of the s-process

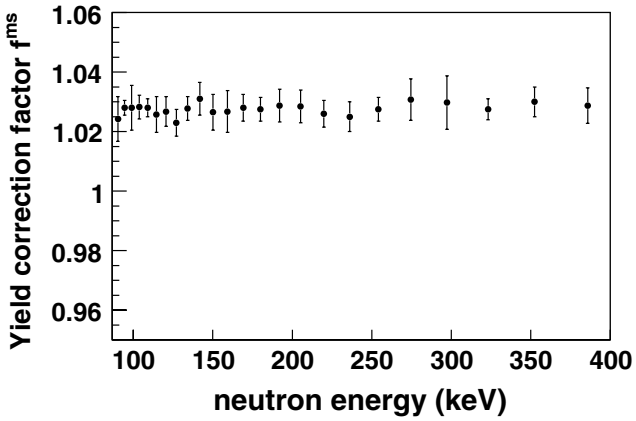

FIG. 2. Correction factor $f^{\rm ms}(E_n)$ due to self-absorption and multiple scattering calculated with the code SESH [21].

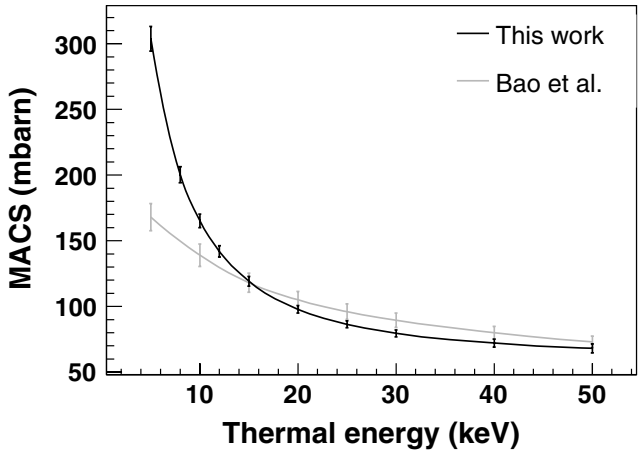

FIG. 3. Maxwellian averaged cross section for ^{204}Pb compared with data from Ref. [22].

path (see Sec. I), nor by the radiogenic contribution due to the decay of the long lived U/Th isotopes. Hence, the ^{204}Pb abundance is determined by the strong temperature and neutron density variations characteristic of the thermal pulses in AGB stars.

The capture cross section measured in this work was convoluted with a Maxwell-Boltzmann distribution in order to determine the Maxwellian averaged cross section (MACS) versus thermal energy (see Table V), which is the relevant input quantity for nucleosynthesis calculations. The MACSs obtained in the present work are compared in Fig. 3 with the values reported in Ref. [22], which are based on the only previous capture measurement [10,23]. The large discrepancy of almost a factor of two below $kT = 15$ keV is due to the resonances below $E_n = 2.5$ keV, which had not been reported before. At higher thermal energies the two data sets are in better agreement. Nevertheless, the present results are consistently smaller and about a factor of two more accurate. About 20% of the MACS at 30 keV is due to the contribution of the average capture cross section beyond 100 keV, reported in Table IV.

The impact of the new MACS in the determination of the s-process abundances N_s was estimated using the stellar model described in Ref. [1]. Calculations have been made for stellar masses of $M = 1.5M_\odot$ and $3M_\odot$, and for a combination of metallicities, [Fe/H] $= -0.3$ and [Fe/H] $= -1.3$, which have been shown to account for the main and strong s-process components, respectively [2,3]. In spite of the much larger MACS at lower stellar temperature, the calculation based on the new cross section yields only a 4.6% lower s-process production of ^{204}Pb , when compared to the same calculation made with the MACS of Ref. [22]. This result clearly illustrates that the production of ^{204}Pb is mostly efficient at the higher temperatures during He-shell flashes, when the decay of ^{204}Tl is strongly enhanced [24].

The present estimate for the s-process abundance of ^{204}Pb at the epoch of solar system formation is 95% (relative to ^{150}Sm). The uncertainty on the solar abundance of lead is as high as 7.8% according to Anders and Grevesse [25], rounded to 10% by Lodders [26]. Within this uncertainty, which applies entirely

TABLE III. Resonance parameters derived from the R-matrix analysis of the ^{204}Pb(n,γ) data.

$E_\circ$ (eV)	l	J	Γ_γ (meV)	$\Delta\Gamma_\gamma$ (%)	Γ_n (meV)	K_r (meV)	ΔK_r (%)
480.3	1	1/2	1.33	4	3.0	0.92[a]	2.7
1333.8	1	1/2	105	4	46.3[b]	32.1[a]	1.3
1687.1	0	1/2	1029	0.7	3340	787[a]	0.5
2481.0	0	1/2	514	1.1	5470	470[a]	1.0
2600.0						8.35	6
2707.1	1	3/2	31.2	9	11.5	16.8	2
3187.9	0	1/2	316	10	1.7	1.69	0.1
3804.9	1	1/2	280	8	66.4	53.7	1.6
4284.1	1	3/2	111	9	24.0	39.4	1.7
4647.5						2.57	9
4719.4	1	3/2	41.2	5	95.0	57.5	3
5473.2	1	1/2				79.0	1.6
5561.4		(1/2)	1.03	10	1.9	0.67	6.4
6700.5	0	1/2	312	3	4540	292	3
7491.0						19.0	0.5
8357.4	0	1/2	1286	1.9	45000	1250	1.9
8422.9						11.3	7
8949.6						22.9	3
9101.0		(1/2)	193	8	150	84.4	4
9649.3	0	1/2	1076	2	7860	946	2
10254						37.0	8
11366	1	3/2	39.0	10	226	66.5	9
11722						22.8	9
12147						54.4	8
12519						24.3	9
12909	0	1/2	569	4	54600	563	4
13007						6.07	10
13382	1	3/2	55.1	10	232	89.0	8
14377						47.8	10
14822	0	1/2	548	4	4301	486	4
15947	1	1/2	201	10	130	79.0	4
16077						16.2	10
16121						66.0	8
16493						19.9	10
17433						39.3	9
17455	1	1/2	528	9	260	174	3
17647	1	3/2	62	0.0	440	109	0.0
18092						31.7	9
18299						19.1	10
18511	1	1/2	362	9	259	151	4
18597						10.1	10
18677						9.52	10
18806	0	1/2	81.3	9	230	60.0	7
19748	0	1/2	738	6	2530	571	4
20396	1	1/2				92.6	8
20776	1	1/2	202	9	300	121	5
20979						41.0	9
21178						43.1	9
21659	1	1/2	258	8	630	183	6
22061						77.1	9
22209	0	1/2	463	6	56833	459	6
23031						21.7	10
23290	1	3/2	99.0	10	1245	183	9
23379						55.1	9
23968						111	8

TABLE III. *(Continued.)*

$E_\circ$ (eV)	l	J	Γ_γ (meV)	$\Delta\Gamma_\gamma$ (%)	Γ_n (meV)	K_r (meV)	ΔK_r (%)
24158	0	1/2	126	10	77300	126	10
24184						124	10
24510		(1/2)	73.0	10	450	62.8	8
25446						118	8
25711						117	8
25805						76.6	9
25914	1	1/2	75.7	10	710	68.4	9
26241						171	9
26665						83.2	9
27207						90.2	9
27410						200	7
27590	0	1/2	747	6	30300	729	6
27884	0	1/2	429	7	6162	401	7
28144	1	1/2	129	9	950	114	8
28950		(1/2)	179	10	330	116	6
29043	1	1/2	100	9	1040	91.6	8
29222						87.1	9
29565						84.5	9
29671	1	1/2	185	9	1250	161	8
30302						220	7
31200						90.0	9
31487		(1/2)	276	10	300	144	5
32647						348	6
32853	0	1/2	781	7	43934	767	7
33504	1	1/2	144	10	1360	130	9
33708	1	1/2	47.7	10	1000	45.5	10
33946	0	1/2	448	9	1380	338	7
34234	1	3/2	81.0	9	8268	160	9
35696						200	8
35981						267	7
36797	1	1/2	30.0	10	4360	29.8	10
37720	1	3/2	103	10	325	156	7
38455						123	8
38732	1	3/2	52	9	855	98.5	9
38977	1	1/2	230	9	1840	204	8
39557	0	1/2	1361	6	158000	1349	6
39890	1	1/2	131	10	2780	125	9
40520	1	1/2	250	9	1230	207	8
40888	1	3/2	270	9	545	361	6
41670	0	1/2	221	9	7050	214	9
42380	1	3/2	182	9	1835	331	8
42496	1	1/2	58	10	7580	57.8	10
42962	0	1/2	570	8	46300	563	8
43080	1	3/2	70	10	2590	136	10
43725	1	1/2	189	10	2670	177	9
43938	1	3/2	2520	10	355	622	1.2
44471	1	1/2	170	10	920	144	8
44950	0	1/2	467	9	21409	457	8
45370	0	1/2	353	9	2780	313	8
45527						406	8
45886	1	1/2	107	10	6220	105	10
46263	1	3/2	283	8	2885	515	8
46700						152	9
47453						237	9
47880	1	3/2	212	9	2520	392	8
49306	0	1/2	453	9	59400	622	1.2

TABLE III. *(Continued.)*

$E_\circ$ (eV)	l	J	Γ_γ (meV)	$\Delta\Gamma_\gamma$ (%)	Γ_n (meV)	K_r (meV)	ΔK_r (%)
50229	1	1/2	221	10	1900	198	9
50490						215	8
50827						321	7
51250						46.5	10
51581	1	1/2	73.6	10	3260	71.9	10
52809	1	3/2	158	9	510	241	7
54260	1	1/2	75.0	10	1880	72.1	10
54476	1	1/2	352	9	3251	318	8
55118	0	1/2	420	9	153000	419	9
55857	1	1/2	163	10	2260	152	9
56084	1	3/2	428	10	500	461	5
56397		(1/2)	431	9	1460	333	7
57179	0	1/2	392	9	36100	388	9
57310						450	5
58266	1	3/2	686	9	1300	898	6
58674						302	8
59334	0	1/2	548	9	4900	493	8
59491	1	(1/2)	1029	10	820	456	4
59717	1	3/2	123	10	4467	239	9
60135	0	1/2	312	10	93980	311	10
61500						196	8
62635	1	3/2	453	9	1000	624	6
62648		(1/2)	100	10	350	78.5	8
63156		(1/2)	212	10	2180	194	9
63492		(1/2)	2690	9	1770	1068	4
63854		(3/2)	275	9	6864	529	9
64002	1	1/2	213	10	2100	193	9
64500						231	8
64925						502	5
65480	0	1/2	570	9	10000	540	8
67122	0	1/2	444	9	13400	429	9
68395						333	6
68882						369	6
69191						383	6
69870	1	3/2	134	10	10000	265	10
70055	1	1/2	2494	10	1000	714	3
71294						328	7
71477						367	6
72249	1	3/2	1136	9	1755	1379	5
73885	0	1/2	963	8	41800	941	8
74683	0	1/2	721	9	149990	718	9
75456						995	0.1
78323	0	1/2	399	10	68001	397	9
79547	1	3/2	172	10	8400	338	9
80540	0	1/2	1268	8	64015	1244	8
82256	0	1/2	989	9	55707	972	8
83940	1	3/2	137	10	19700	271	10
84334	0	1/2	1033	9	8480	921	8
84980		(1/2)	988	9	4930	823	8
86013		(1/2)	1074	9	3000	791	7
86765	0	1/2	1554	9	258129	1545	8
88071	0	1/2	1058	9	43200	1033	9
89052	1	3/2	447	9	21202	875	9
90794	0	1/2	1348	9	26700	1283	8
91530	1	3/2	941	9	2000	1279	6
92323	0	1/2	531	10	143985	529	10

TABLE III. *(Continued.)*

$E_\circ$ (eV)	l	J	Γ_γ (meV)	$\Delta\Gamma_\gamma$ (%)	Γ_n (meV)	K_r (meV)	ΔK_r (%)
93561	0	1/2	505	10	136012	503	9
95080	2	3/2	982	9	6601	1710	7
96298	1	3/2	1021	8	7850	1808	7
98123	1	3/2	274	10	23351	543	9

[a]First determination in a capture experiment.
[b]Neutron width fitted as $\Gamma_n = 46.3 \pm 2.5$ meV.

to the solar s-process contribution of ^{204}Pb, the s-process abundance of ^{204}Pb obtained here is in perfect agreement with the expected value of 100%.

A more consistent result will be attempted in a comprehensive study [27] based on more stellar detailed model calculations and on a complete set of new cross sections in the Pb/Bi region, e.g., recent data for ^{207}Pb [28] and ^{209}Bi [15] and new data for ^{206}Pb.

VII. SUMMARY

The neutron capture cross section of ^{204}Pb has been measured in a high resolution time-of-flight experiment at the CERN n_TOF facility. Data were obtained in the neutron energy range from 1 eV to 440 keV. From a resonance analysis with the R-matrix code SAMMY the capture widths of 170 resonances have been determined between 400 eV and 100 keV with an overall systematic uncertainty of 3%. The average capture cross section in the energy interval from 100 to 440 keV was determined with an uncertainty of ∼10%. From these results, Maxwellian averaged cross sections have been derived(see Table V), which exhibit large discrepancies with respect to previous data. At thermal energies below $kT = 15$ keV the present values are larger by up to a factor of two because new low-energy resonances have been included, whereas they are systematically lower by about 10% at high values of kT, presumably because the neutron sensitivity of the older data had been underestimated. In any case, the systematic uncertainty on the MACS has been improved by a factor of two when compared to the values reported in Ref. [22]. In spite of the significantly higher stellar cross sections at low kT, stellar model calculations show that the ^{204}Pb abundance is not affected by more than 5%. This result indicates that the production of ^{204}Pb takes place during He-shell flashes, where the cross section differences with respect to the previous measurement are smaller and where the comparably high temperatures lead to an enhancement in the β-decay rate of ^{204}Tl, thus favoring the s-process path towards ^{204}Pb.

TABLE IV. Average neutron capture cross section for ^{204}Pb.

E_{low} (keV)	E_{high} (keV)	Cross section (barn)	Statistical uncertainty[a] (%)
88.210	92.404	0.059	9
92.404	96.748	0.059	5
96.748	101.406	0.058	11
101.406	106.408	0.057	8
106.408	111.790	0.057	7
111.790	117.591	0.056	8
117.591	123.855	0.056	7
123.855	130.634	0.055	7
130.634	137.985	0.054	6
137.985	145.974	0.054	6
145.974	154.678	0.053	6
154.678	164.185	0.053	7
164.185	174.596	0.052	7
174.596	186.030	0.051	6
186.030	198.625	0.051	5
198.625	212.544	0.050	5
212.544	227.981	0.049	5
227.981	245.162	0.049	5
245.162	264.363	0.048	4
264.363	285.911	0.047	4
285.911	310.207	0.046	4
310.207	337.739	0.046	4
337.739	369.107	0.045	4
369.107	405.060	0.044	4
405.060	443.512	0.043	3

[a]This value has to be added in quadrature with the overall systematic uncertainty of 10%.

TABLE V. Maxwellian averaged cross section for ^{204}Pb.

Thermal energy kT (keV)	MACS (mbarn)
5	304(9)
8	200(6)
10	165(5)
12	142(4)
15	119(4)
20	98(3)
25	86(3)
30	79(3)
40	72(3)
50	68(3)

ACKNOWLEDGMENTS

This work was supported by the European Commission (FIKW-CT-2000-00107), by the Spanish Ministry of Science and Technology (FPA2001-0144-C05), and partly by the Italian MIUR-FIRB grant "The astrophysical origin of the heavy elements beyond Fe."

[1] C. Arlandini, F. Käppeler, K. Wisshak, R. Gallino, M. Lugaro, M. Busso, and O. Straniero, Astrophys. J. **525**, 886 (1999).

[2] C. Travaglio, D. Galli, R. Gallino, M. Busso, F. Ferrini, and O. Straniero, Astrophys. J. **521**, 691 (1999).

[3] C. Travaglio, R. Gallino, M. Busso, and R. Gratton, Astrophys. J. **549**, 346 (2001).

[4] U. Ratzel, C. Arlandini, F. Käppeler, A. Couture, M. Wiescher, R. Reifarth, R. Gallino, A. Mengoni, and C. Travaglio, Phys. Rev. C **70**, 065803 (2004).

[5] J. J. Cowan, F.-K. Thielemann, and J. W. Truran, Phys. Rep. **208**, 267 (1991).

[6] J. J. Cowan, B. Pfeiffer, K.-L. Kratz, F.-K. Thielemann, C. Sneden, S. Burles, D. Tytler, and T. C. Beers, Astrophys. J. **521**, 194 (1999).

[7] H. Schatz, R. Toenjes, B. Pfeiffer, T. C. Beers, J. J. Cowan, V. Hill, and K.-L. Kratz, Astrophys. J. **579**, 626 (2002).

[8] K.-L. Kratz, B. Pfeiffer, J. J. Cowan, and C. Sneden, New Astron. Rev. **48**, 105 (2004).

[9] R. Gallino, C. Arlandini, M. Busso, M. Lugaro, C. Travaglio, O. Straniero, A. Chieffi, and M. Limongi, Astrophys. J. **497**, 388 (1998).

[10] D. J. Horen, R. L. Macklin, J. A. Harvey, and N. W. Hill, Phys. Rev. C **29**, 2126 (1984).

[11] U. Abbondanno *et al*., Tech. Rep. CERN-SL-2002-053 ECT (2003).

[12] R. Plag, M. Heil, F. Käppeler, P. Pavlopoulos, R. Reifarth, and K. Wisshak, Nucl. Instrum. Methods Phys. Res. A **496**, 425 (2003).

[13] U. Abbondanno *et al*., Nucl. Instrum. Methods Phys. Res. A **521**, 454 (2004).

[14] R. Macklin, J. Halperin, and R. Winters, Nucl. Instrum. Methods Phys. Res. A **164**, 213 (1979).

[15] C. Domingo-Pardo *et al*., Phys. Rev. C **74**, 025807 (2006).

[16] C. Borcea *et al*., Nucl. Instrum. Methods Phys. Res. A **513**, 524 (2003).

[17] S. Marrone *et al*., Nucl. Instrum. Methods Phys. Res. A **517**, 389 (2004).

[18] R. L. Macklin and J. H. Gibbons, Phys. Rev. **159**, 1007 (1967).

[19] S. F. Mughabghab, *Neutron Cross Sections: Neutron Resonance Parameters and Thermal Cross Sections* (Academic Press, New York, 2006).

[20] N. M. Larson, "Updated users' guide for SAMMY: Multilevel R-matrix fits to neutron data using Bayes' equations," SAMMY, computer code Report ORNL/TM-9179/R7, Oak Ridge National Laboratory (2006).

[21] F. H. Fröhner, SESH computer code, GA-8380, Gulf General Atomic (1968).

[22] Z. Y. Bao, H. Beer, F. Käppeler, F. Voss, K. Wisshak, and T. Ranscher, At. Data Nucl. Data Tables **76**, 70 (2000).

[23] B. Allen, R. Macklin, R. Winters, and C. Fu, Phys. Rev. C **8**, 1504 (1973).

[24] K. Takahashi and K. Yokoi, At. Data Nucl. Data Tables **36**, 375 (1987).

[25] E. Anders and N. Grevesse, Geochim. Cosmochim. Acta **53**, 197 (1989).

[26] K. Lodders, Astrophys. J. **591**, 1220 (2003).

[27] S. Bisterzo, R. Gallino, F. Käppeler, and C. Domingo-Pardo (in preparation).

[28] C. Domingo-Pardo *et al*., Phys. Rev. C **74**, 055802 (2006), nucl-ex/0610039.